ACS APPLIED BIO MATERIALS

www.acsabm.org

Forum Article

Computational Insights into Prostaglandin E_2 Ligand Binding and Activation of G-Protein-Coupled Receptors

Nam P. Vu,[⊥] Luke Ali,[⊥] Theresa L. Chua, Daniel A. Barr,* Heidi P. Hendrickson,* and Dhara J. Trivedi*

Cite This: https://doi.org/10.1021/acsabm.2c01049

Read Online

ACCESS | Metrics & More | Article Recommendations | Supporting Information

ABSTRACT: G-protein coupled receptors (GPCRs) are eukaryotic integral membrane proteins that regulate signal transduction cascade pathways implicated in a variety of human diseases and are consequently of interest as drug targets. For this reason, it is of interest to investigate the way in which specific ligands bind and trigger conformational changes in the receptor during activation and how this in turn modulates intracellular signaling. In the present study, we investigate the way in which the ligand Prostaglandin E2 interacts with three GPCRs in the E-prostanoid family: EP1, EP2, and EP3. We examine information transfer pathways based on long-time scale molecular dynamics simulations using transfer entropy and betweenness centrality to measure the physical transfer of information among residues in the system. We monitor specific residues involved in binding to the ligand and investigate how the information transfer behavior of these residues changes upon ligand binding. Our results provide key insights that enable a deeper understanding of EP activation and signal transduction functioning pathways at the molecular level, as well as enabling us to make some predictions about the activation pathway for the EP1 receptor, for which little structural information is currently available. Our results should advance ongoing efforts in the development of potential therapeutics targeting these receptors.

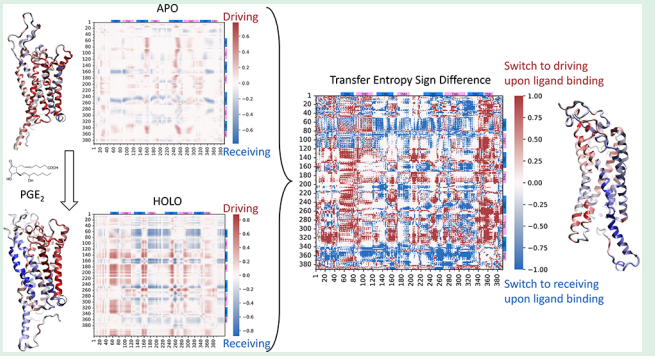

KEYWORDS: *G-protein coupled receptors, transduction cascade pathways, therapeutics, transfer entropy*

INTRODUCTION

Prostaglandin E_2 (PGE_2) is a prostanoid molecule that contributes to diverse physiological functions, including immune responses, bone formation, cardiovascular protection, inflammatory processes, and reproductive activity,[1] through its interaction with E-prostanoid (EP) G-protein-coupled receptors (GPCRs) EP1, EP2, EP3, and EP4.[2,3] GPCRs are proteins that are situated in the cell membrane by their characteristic seven transmembrane helices, and their major function is to transmit an extracellular signal (e.g., made by a small molecule, a photon, etc.) to the inside of a cell (Figure 1), which makes GPCRs an excellent target for pharmaceuticals.[4,5] A GPCR is coupled to a G-protein inside the cell, and upon GPCR activation the G-protein complex will dissociate, which in turn sets off signaling cascades within the cell.

The activation of the EP GPCRs leads to the transduction of distinct signaling pathways specific to each receptor. For three of these EP receptors, experimental crystal and cryo-EM structures enabled detailed structural insight into potential mechanisms for activating these pathways, however the structure of EP1 remains unknown.[6−9] While there are similarities across the EP receptors, it was found that the activation of EP2 differs somewhat from those of other GPCRs.[9] For example, a common activation mechanism involved in Family A GPCRs, including EP3, is the Trp toggle switch (i.e., transmission switch, CWXP) mechanism. In this mechanism, a ligand interaction with $W^{6.48}$ and subsequent change in orientation enables the cytoplasmic end of transmembrane helix 6 (TM6) to shift outward and the extracellular end of the TM region to shift inward.[4,10] However, EP2 does not have the conserved $W^{6.48}$ and activation is thought to proceed through hydrophobic contacts between $M124^{3.40}$, $I208^{5.49}$, $F273^{6.44}$, and $L304^{7.41}$.[9] Variation among activation mechanisms across the EP receptor subtypes means that elucidating the activation pathways specific to each agonist, receptor, and coupled G-protein complex, especially in EP1 where the structure is unknown, remains a challenge.[11]

When investigating EP receptor activation, it is of interest to characterize the way in which PGE_2 affects information flow in the receptor in order to develop more effective therapeutics

Special Issue: Computational Advances in Biomaterials

Received: December 18, 2022
Accepted: April 3, 2023

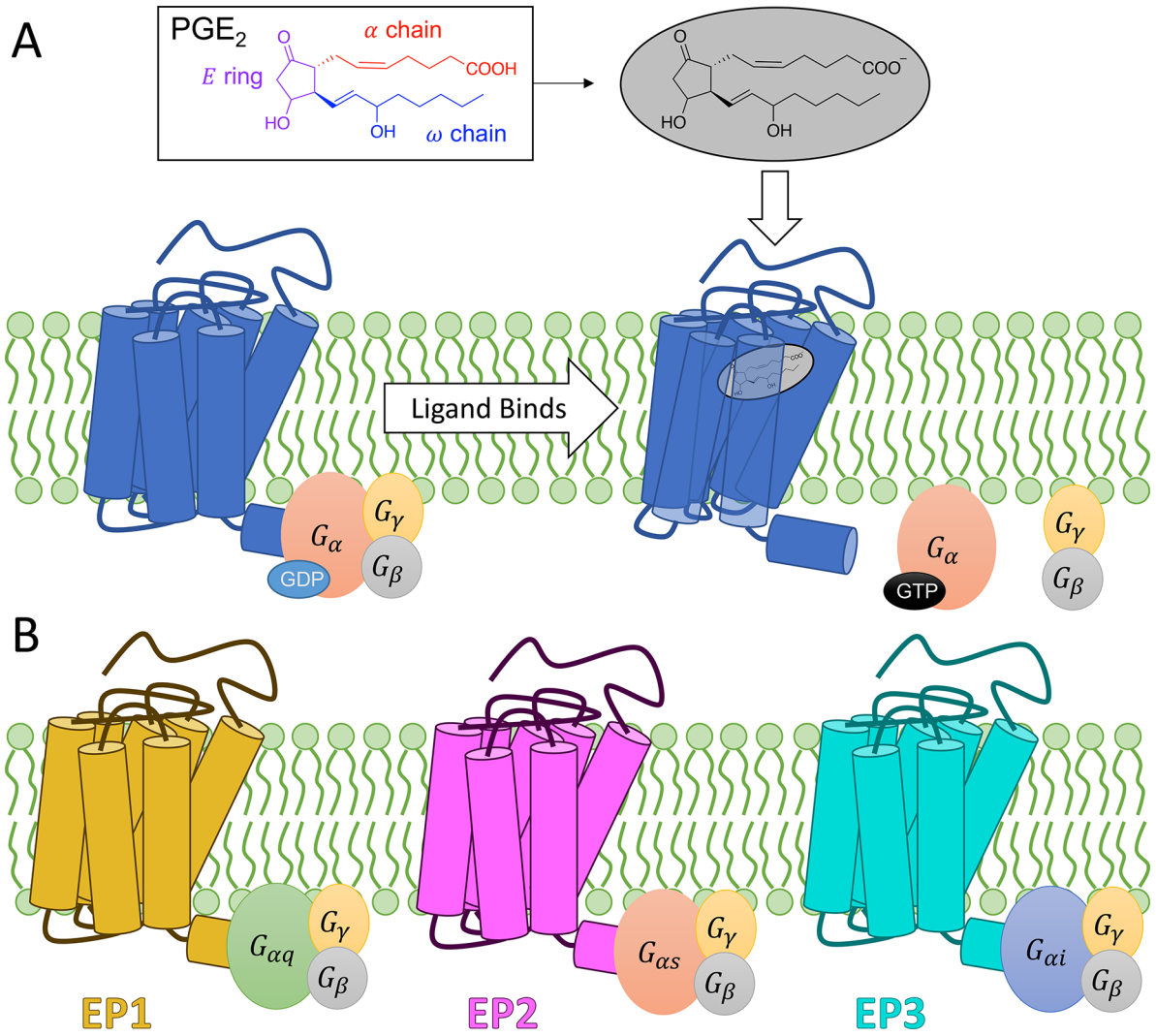

Figure 1. (A) Schematic illustration of a GPCR activated by a small molecule ligand (PGE2). Upon ligand binding, the Gα subunit releases GDP, enabling GTP to bind, and the Gβ and Gγ subunits dissociate from Gα. The structure of PGE_2 is provided in the top panel of the figure. (B) Schematic illustration of EP1 (mustard), EP2 (magenta), and EP3 (cyan) and the primary Gα subunits to which they are coupled.

specific to each receptor.[12−14] The signal transmission from one site of a protein to another site, influencing the activity of that site, is known as allosteric communication.[15,16] This mechanism operates over a mechanical pathway that can be studied quantitatively by implementing transfer entropy (TE) approaches.[17] Such approaches allow for in-depth analysis of residue motion with the goal of quantifying residue−residue communication.[18,19] In addition, methods of this type may be promising when looking at the overall pathway along which the information travels.[16] The results of this method provide deeper insights into the ways that each residue of the protein is affected by the other residues in the protein, thereby giving us a quantitative way to measure the amount of information transferred between two allosteric sites. It is of particular interest to examine changes in transfer entropy (or information transfer behavior) in the protein as a whole and in specific functional residues before and after a biologically relevant transition (e.g., phosphorylation, ligand binding, etc.).[16,20]

The specific EP receptors are each coupled with different G-proteins that have distinctive signaling pathways.[2] The EP1 receptor is known to be involved in regulation of calcium ion concentration and inducing smooth muscle contraction through interaction with the $G_{\alpha q}$ protein: when the endogenous ligand PGE_2 binds to the EP1 receptor, it triggers intracellular Ca^{2+} levels to rise.[21,22] The EP2 receptor binds to the $G_{\alpha s}$ protein and is involved in increasing cyclic adenosine monophosphate (cAMP) levels involved in smooth muscle relaxation. Interestingly, the EP2 receptor is thought to also have a signal transduction pathway that operates independently of any G-protein.[23] EP3 receptor activation triggers reduction in cAMP levels which inhibits the relaxation of smooth muscle tissue through binding to the $G_{\alpha i}$ protein.[21,24] The EP4 receptor is involved in vascular relaxation as well as in the formation of new blood vessels.[22] The EP4 receptor resembles the action of the EP2 receptor in such that it binds to the $G_{\alpha s}$ protein and is positively coupled to adenylate cyclase.[21] Although recently published experimental structures of the EP2, EP3, and EP4 receptors have provided a wealth of information about EP activation mechanisms, the complete picture of activation and information transfer in EP receptors, especially in EP1, remains an active area of research.[6−9]

In this paper, we present a systematic study of the behavior of the EP1, EP2, and EP3 receptors with the use of transfer entropy approaches to provide deeper understanding of the mechanisms

https://doi.org/10.1021/acsabm.2c01049
ACS Appl. Bio Mater. XXXX, XXX, XXX−XXX

that facilitate the information transfer from the ligand binding site on the respective EP receptor to the intracellular site where the initiation of signal cascade occurs. We study the residue−residue communication by analyzing long-time scale molecular dynamics (MD) simulation trajectories. The transfer entropy is extracted from the variance-covariance matrix obtained from the analysis of alpha-carbon (CA) fluctuations, and can be used to characterize the "driving" and "responding" nature of each residue in the protein, as well as the change in information transfer upon ligand binding. We further compared residues across the different receptors to gain a better understanding of role of residues within EP receptors in the information transfer process. The investigation thus provides molecular-level insights to the binding and activation process of the PGE_2 ligand with GPCRs.

METHODS

System Preparation and MD Simulations. The complete structures of original, inactive prostaglandin receptors EP1, EP2 and EP3 were obtained from AlphaFold (Figure S1),[25,26] with UniProt accession numbers P34995, P43116, and P43115 respectively. AlphaFold structures were selected in order to model the full protein sequence for each receptor. Details regarding the alignment between AlphaFold and experimental EP2 and EP3 structures are provided in Table S1. The sequences were aligned (Table S1) using the G-protein Database[27] in order to assign Ballesteros-Weinstein[28] (BW) numbering scheme to each residue. The numbering scheme is provided in the Supporting Information (Table S2). The receptors were capped with zwitterionic terminal groups. The protein was placed in a phospholipid bilayer with a composition of 90% POPC: 10% CHOL using the lipid21 force field,[29] and was solvated in a box of OPC water[30] extended 15 Å with 150 mM NaCl using packmol-memgen.[31] The PGE_2 ligand was prepared by first aligning the AlphaFold structures to the reported experimental structures of active receptors acquired from Protein Data Bank (access codes for EP2 and EP3, respectively, are 7CX2[9] and 6AK3[7]), then combining the PGE_2 ligand from the experimental structure with the apo AlphaFold structure to create holo model systems. For the holo EP1 model, the PGE_2 ligand was extracted from the EP3 crystal structure. This choice was made because both EP1 and EP3 have been shown to bind to the $G_{\alpha i}$ (secondary for EP1) and $G_{\alpha q}$ (secondary for EP3) proteins, unlike EP2, which bind to $G_{\alpha s}$ (primary) and $G_{\alpha q}$ (secondary) proteins.[2,23] The alignment was carried out for all atoms using the align feature in PyMOL[32] with RMSD provided in the Supporting Information (Table S1). Gaussian16[33] and GaussView6[34] were used to add hydrogens to the ligand and minimize energy, while antechamber[35] was used to assign force field parameters to the ligand using the general force field gaff2.[36] The ligand force field parameter file is provided in the Supporting Information. The PGE_2 ligand was simulated in the anionic, carboxylate form.

All systems were constructed using LEaP (part of AmberTools[37]) using the protein force field protein.ff19SB,[38] general force field gaff2,[36] lipid21[29] force field, and OPC[30] force field for water and ions; all simulations were performed using AMBER22.[37] The system was equilibrated following the procedure described in the AMBER-Membrane Protein Tutorial by C. J. Dickson.[39] First, a short minimization step was performed with CPU-version pmemd, then a longer minimization step and all following steps were run with GPU-version pmemd.cuda. Heating of the system occurred in two steps, one 5 ps-long up to 100 K, and another 100 ps-long up to 303 K. This was followed by a 1 ns-long NPT (constant temperature, constant pressure) equilibration with restraints on the receptors' backbone atoms (and PGE_2 ligand heavy atoms, for holo complexes) throughout a 1 ns-long NPT equilibration with Cartesian weights set at 5 kcal mol^{-1} $Å^{-2}$; another 1 ns-long NPT equilibration was then performed with the same restraints but only on alpha-carbon (CA) atoms (and PGE_2 ligand heavy atoms, for holo complexes). Next, all constraints were removed for a 100 ns-long NPT equilibration. Finally, a 0.5 μs-long NPT production run utilized Monte Carlo barostat and hydrogen mass repartitioning.[40] The nonbonded cutoffs were chosen to be 10 Å in all steps. SHAKE[41] was applied to constrain bonds involving hydrogen atoms, and Langevin's thermostat was used with a collision frequency of 1.0 ps^{-1} to maintain the temperature of 303 K. Snapshots were saved every 10 ps, and only the simulation trajectories from the final production step were used for analysis. The resulting trajectories were aligned and analyzed with CPPTRAJ[42] as part of AMBER22, VMD,[43] and the MDAnalysis[44,45] package in Python; the structures were visualized with VMD,[43] PyMOL,[32] and Flare.[46−49] Convergence of the simulations was assessed by plotting the total energy (Figure S2) and per-residue root-mean-square fluctuations (RMSF) (Figure S3).[50] The per-residue RMSF measures the fluctuations of each α carbon from its average position during the simulation. As shown in Figure S3, the larger fluctuations are localized to the loop regions and not the transmembrane helices. Residues that were within 3 Å of the PGE_2 ligand for more than 75% of the trajectory were considered to be relevant residues in the ligand binding site. The HBonds plugin in VMD was used to determine which residues form hydrogen bonds with PGE_2 during the simulation, where two heavy atoms were considered to participate in a hydrogen bond within a distance cutoff of 3.0 Å and angle cutoff of 20°.

Transfer Entropy Calculations. All analyses were based on the position of the alpha- carbon (CA) atoms of each residue over the duration of the last production step, using MDAnalysis[44,45] package in Python. The input for variance-covariance and transfer entropy analysis is calculated by the fluctuation of each CA atom with respect to the average position over time. Pearson correlation coefficients were used to quantify linear correlations of allosteric communication between the residues. More detailed information can be found in works by Garcia Michel et al.[16] Here, we restate the relevant highlights for clarification. Specifically, for the system with n CA atoms, by denoting the time-dependent position of the ith CA atom in vector X_i having average position $\bar{X}_i$, the variance-covariance matrix of fluctuations is defined by the symmetric, positive semidefinite $n \times n$ matrix C where

$$C_{ij} = (X_i - \bar{X}_i)(X_j - \bar{X}_j) \tag{1}$$

Satisfactory convergence of the variance-covariance matrix C was obtained using a block analysis approach (Figure S4).[18,51,52] The matrix of Pearson correlation coefficients of C are diagonalized wherein

$$Cov(C) = U\Lambda U^{-1} \tag{2}$$

such that only the frequencies of motions with eigenvalues $\lambda_i > 0.01$ in Λ were retained. Following the dynamic Gaussian Network Model (dGNM) method, the transfer entropy from CA atom i to atom j is calculated as described by Hacisuleyman and Erman:[53]

$$\begin{aligned} T_{i\to j}(\tau) = {} & \frac{1}{2}\ln\left((\Sigma_k A_{jj}(k))^2 - \left(\Sigma_k A_{jj}(k)\exp\left(-\frac{\lambda_k\tau}{\tau_0}\right)\right)^2\right) \\ & - \frac{1}{2}\ln\Bigg[(\Sigma_k A_{ii}(k))(\Sigma_k A_{jj}(k))^2 + 2(\Sigma_k A_{ij}(k))\Sigma_k A_{jj}(k) \\ & \exp\left(-\frac{\lambda_k\tau}{\tau_0}\right)\Sigma_k A_{ij}(k)\exp\left(-\frac{\lambda_k\tau}{\tau_0}\right) \\ & - \left\{\left(\Sigma_k A_{ij}(k)\exp\left(-\frac{\lambda_k\tau}{\tau_0}\right)\right)^2 + (\Sigma_k A_{ij}(k))^2\right\}(\Sigma_k A_{jj}(k)) \\ & - \left(\Sigma_k A_{jj}(k)\exp\left(-\frac{\lambda_k\tau}{\tau_0}\right)\right)^2(\Sigma_k A_{ii}(k))\Bigg] \\ & - \frac{1}{2}\ln[(\Sigma_k A_{jj}(k))] \\ & + \frac{1}{2}\ln[(\Sigma_k A_{ii}(k))(\Sigma_k A_{jj}(k)) - (\Sigma_k A_{ij}(k))^2] \end{aligned} \tag{3}$$

https://doi.org/10.1021/acsabm.2c01049
ACS Appl. Bio Mater. XXXX, XXX, XXX−XXX

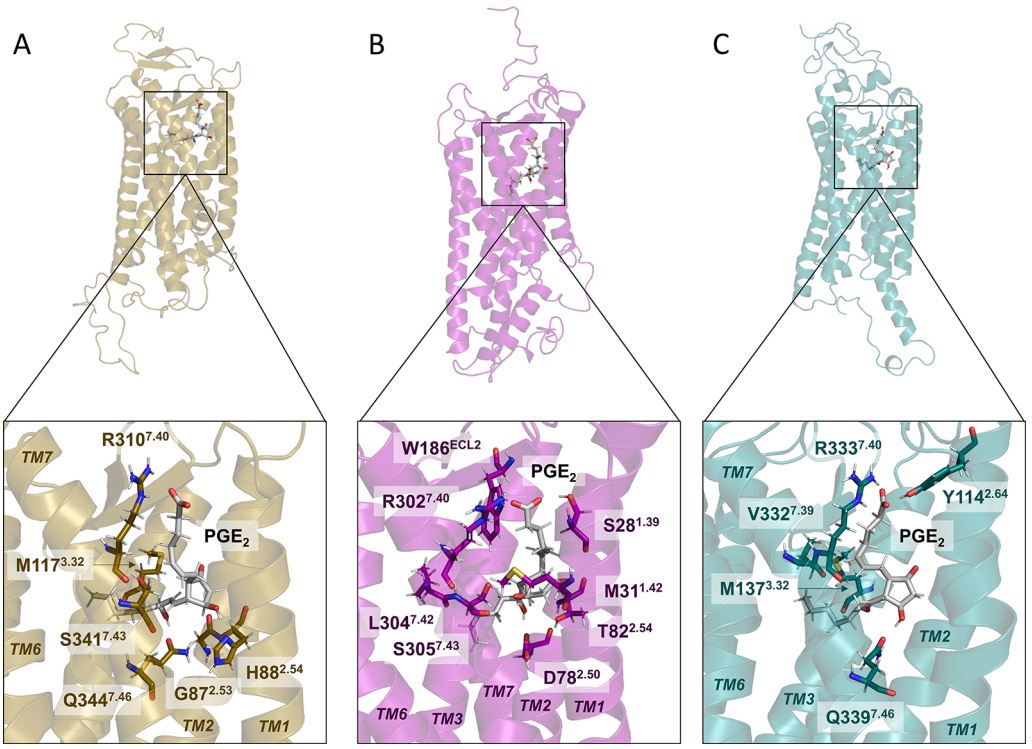

Figure 2. Equilibrated structures and relevant residues for (A) EP1, (B) EP2, and (C) EP3. The PGE_2 ligand is shown as sticks (gray). The lower panels show zoomed-in views of the region around the ligand binding site for each receptor with residues that are within ≲3 Å of PGE_2 for >75% of the trajectory shown as sticks.

where $n \times n$ matrix A, depending on the kth eigenvalue $\lambda_k \in \Lambda$, is defined by the product of the ith and jth component of the kth eigenvector in U,

$$A_{ij}(k) = \lambda_k^{-1} u_i(k) u_j(k) \tag{4}$$

Finally, the directional normalized transfer entropy (DNTE) from residue i and j is the difference of the normalized transfer entropy from i to j and normalized entropy transfer from j to i:

$$DNTE_{i\to j} = (\tilde{T}_{i\to j}) - (\tilde{T}_{j\to i}) \in [-1, 1] \tag{5}$$

Contextually, DNTE implies the magnitude and direction of information flow: $DNTE_{i\to j} = 1$ implies that the net information flow is entirely directed from residue i to residue j (or from j to i for $DNTE_{i\to j} = -1$), while $DNTE_{i\to j} = 0$ indicates the lack of, or equal but opposite, information flow between residues i and j. One way to distinguish between these two cases of low DNTE is to treat the transfer entropy as a directed network[54,55] and calculate the betweenness centrality for each residue. Residues with high TE but low DNTE generally show up with high betweenness, where residues with low TE and low DNTE generally show up with low betweenness. Additionally, residues with high betweenness provide a first level of insight into pathways of information flow through the protein, indicating points of high information throughput between strongly driving and strongly receiving residues. In practice, we use the built-in functions in Mathematica[56] to create the adjacency network and calculate the betweenness centrality for each DNTE matrix in our study.

Because our focus in this work is to study the effect of ligand binding, we calculate the sign difference matrix[18] for each pair of apo/holo DNTE matrices corresponding to each receptor in our study. Each element in the signed difference matrix, SGN wherein

$$SGN_{i\to j} = \begin{cases} 1, & \text{if } DNTE_{i\to j}(apo) > 0 \text{ and } DNTE_{i\to j}(holo) < 0 \\ -1, & \text{if } DNTE_{i\to j}(apo) < 0 \text{ and } DNTE_{i\to j}(holo) > 0 \\ 0, & \text{otherwise} \end{cases} \tag{6}$$

is calculated such that the sign difference matrix will be positive if the DNTE from i to j switches from responding in the apo simulation to driving in the holo simulation and negative otherwise (we note that there are no off-diagonal elements in the DNTE matrix that are equal to zero).

RESULTS AND DISCUSSION

In our simulations of the holo complexes, we find that the PGE_2 ligand remains stable in the receptor and makes durable contacts (≲3 Å heavy atom distance for >75% of the trajectory, Table S3) with residues that have been identified in structural and functional studies as being important for binding and signaling. In all holo complexes, $R^{7.40}$ forms hydrogen bond contacts with the α chain carboxyl group of the PGE_2 ligand, as shown in Figure 2. The hydrogen bond interaction between the carboxyl group and the conserved R is known to be crucial for functional activation of EP receptors.[57] In EP2, residues in TM1, TM2, and TM7 make stable contacts with the ligand (Figure 2B), consistent with the contacts in the experimental structure. In particular, $S28^{1.39}$, $W186^{ECL2}$, and $R302^{7.40}$ form consistent hydrogen bond contacts with the PGE_2 carboxyl group. Residues $T82^{2.54}$ and $S305^{7.43}$ with the carbonyl and hydroxyl groups on the PGE_2 E ring that are known to facilitate the formation of an extended polar network connecting the ligand and the protein and allowing the ligand to move down into the binding pocket.[9] In addition, $L304^{7.42}$ also forms contacts with the ω chain of PGE_2. Residues $D78^{2.50}$ and $W186^{ECL2}$ also form consistent hydrogen bond interactions with the PGE_2 ω chain

https://doi.org/10.1021/acsabm.2c01049
ACS Appl. Bio Mater. XXXX, XXX, XXX−XXX

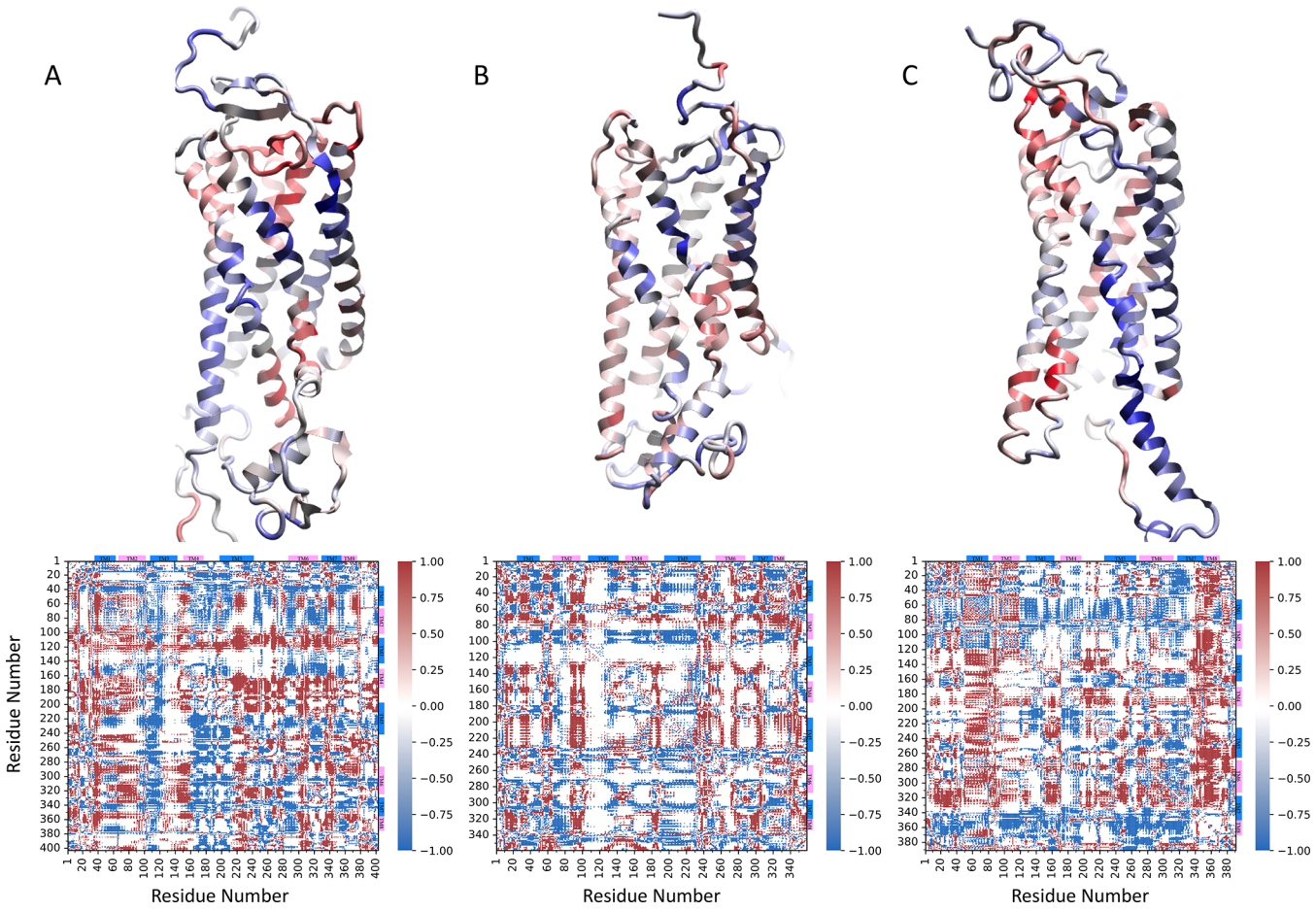

Figure 3. Signed difference matrix (bottom panels) and row-wise sum of each matrix plotted on each receptor (top panels) for (A) EP1, (B) EP2, and (C) EP3. The signed difference matrix (eq 6 in the text) shows the change in information transfer relationship between residues *i* (on the vertical axis) and *j* (on the horizontal axis) upon ligand binding. Positions of transmembrane helices are marked along the top and right axes in blue and pink boxes. For each pair of residues, if ligand binding causes the information transfer to switch direction/sign, a red value indicates that i switches from receiving in the apo state to driving in the holo state; a blue value indicates that residue i switches from driving in the apo state to receiving in the holo state. Residue pairs in white on the signed difference matrix indicate no sign switching upon ligand binding. The row-wise sum of the signed difference matrix provides an overview of the net change in information transfer behavior of each residue upon ligand binding. The results of this sum are visualized on the protein structure in the top panels.

hydroxyl and α chain carboxyl group, respectively. W186^{ECL2} is known to interact with other EP2 agonists and is in proximity to T185^{ECL2}, which is also known to interact with PGE_2.[9] D78$^{2.50}$ forms stable contacts with the ligand during simulations, though not mentioned explicitly in the available literature; however, D$^{2.50}$ is known to interact with PGE_2 in the EP3 receptor.[7]

In EP3, we observe the consistent hydrogen bond interactions between the PGE_2 α chain carboxyl group and residues Y114$^{2.64}$ in addition to R302$^{7.40}$ (Figure 2C). Likewise, M137$^{3.32}$ is also observed to interact with the PGE_2 α chain, in agreement with contacts identified in the crystal structure. Also consistent with the experimental structure, V332$^{7.39}$ was observed to interact with the PGE_2 ω chain. Residue Q339$^{7.46}$ is known to be part of the binding pocket for PGE_2, and here Q$^{7.46}$ was observed to form hydrogen bond contacts with the E ring hydroxyl group.

While there is no experimental structure for EP1, the residues identified as forming consistent contacts are consistent with those observed for EP2 and EP3. As the with other receptors, R338$^{7.40}$ forms hydrogen bonds with the PGE_2 α chain carboxyl group. A hydrogen bond is also observed between the PGE_2 E ring hydroxyl group and H88$^{2.54}$, and G87$^{2.53}$ is also in close proximity to the PGE_2 ligand during the simulation. For EP2, T82$^{2.54}$ interacts with the α chain carboxyl group instead of the E ring hydroxyl group. Similar to EP2, S341$^{7.43}$ is consistently close to the ω chain, however, specific hydrogen bonds are not observed in the EP1 simulation. EP1 also forms contacts similar to those observed in EP3. M117$^{3.32}$ forms consistent interactions with the ω chain. Q344$^{7.46}$ is also a close contact, but it forms a hydrogen bond with the ω chain hydroxyl group instead of the E ring hydroxyl group as in EP3.

We focus our analysis in this work on residues that show significant changes in the sign of the transfer entropy upon ligand binding (see Methods section, above, and Figure 3; absolute TE matrices are provided in Figure S5). In general, we find that in the proximity of the ligand binding pocket, TM1, TM2, and TM7 switch from driving to responding upon ligand binding while TM3, TM4, TM5, and TM6 switch from responding to driving, particularly on the extracellular end, in all three receptors (Figure 3). Most of the residues interacting with the PGE_2 ligand during the simulations were located on TM1, TM2, and TM7, and as in general, these specific residues switch from driving to responding upon ligand binding. For example, R$^{7.40}$ plays an important role in binding to the carboxyl group of the ligand and switches from driving to responding

https://doi.org/10.1021/acsabm.2c01049
ACS Appl. Bio Mater. XXXX, XXX, XXX−XXX

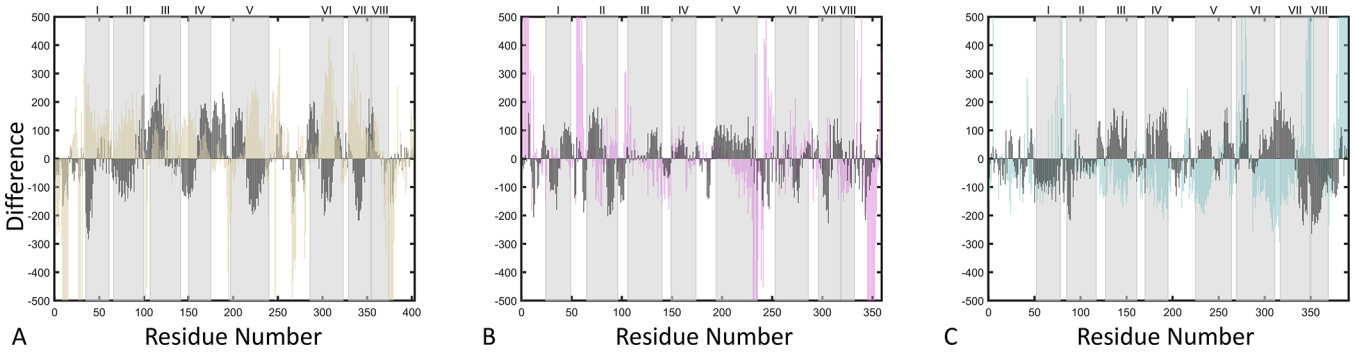

Figure 4. Per-residue difference in betweenness centrality upon ligand binding (holo minus apo) for (A) EP1, (B) EP2, (C) EP3 shown in mustard, magenta, and cyan, respectively. Residues that have greater betweenness centrality in the holo complex show up with positive values, and those with greater betweenness in the apo complex have negative values. The row-wise sum of the signed difference matrix is shown in gray for each complex; residues that predominantly switch from responding to driving upon ligand binding show positive values, residues that switch from driving to responding upon ligand binding show negative values. The positions of each transmembrane helix are shaded in gray and labeled above each plot.

upon ligand binding in all three of our systems. Interestingly, some differences are observed between the receptors for residues that bind PGE_2 in both EP1 and EP3. For example, $M^{3.32}$ switches from responding to driving upon ligand binding, and this shift is more dramatic in both EP1 and EP3 than in EP2. In addition, while $Q^{7.46}$ switches to responding for EP1 and EP3, the corresponding $S^{7.46}$ in EP2 switches to driving.

While the row-wise sum of the signed difference matrix can provide valuable information about a whether a residue is generally driving or responding upon ligand binding, it does not provide the entire story. For example, a residue that is drives information transfer just as much as it responds will have a very low row-wise sum, regardless of the magnitude of information that is transferred through that residue. Thus, in addition to investigating the difference in transfer entropy upon ligand binding, we also investigated the difference in betweenness centrality, as described in the methods.

The change in betweenness centrality that occurs upon ligand binding for each receptor is provided in Figure 4 (betweenness centrality for apo and holo is provided in Figure S6). As shown in the plot there is a general increase in betweenness upon ligand binding for EP1, while for EP3 there is a general decrease. On the other hand, there appears to be a balance between increasing and decreasing betweenness across residues for EP2. To verify these general trends across receptors, the average betweenness change per residue was calculated for residues within the TM region and including Helix 8 (i.e., excluding the N- and C-terminal loops). The averages, provided in Table 1 also show an average increase in betweenness for EP1, no average change for EP2, and an average decrease for EP3.

Examination of the betweenness centrality of individual functional residues provides insight into possible mechanisms of communication by which the signal travels through the protein.

Table 1. Average Per-Residue Difference in Betweenness Centrality upon Ligand Binding (Holo Minus Apo) for EP1, EP2, EP3[a]

Receptor	Average betweenness centrality difference per residue	Residues included in calculation
EP1	62.39	35−374
EP2	0.47	24−332
EP3	−30.01	52−369

[a]Calculations were carried out for residues within the TM region.

In particular, we considered how the betweenness changes for the conserved toggle switch residue $W^{6.48}$ (and associated residues) in EP3 and for the residues involved in the alternative hydrophobic contact mechanism reported for EP2. In Table 2, the difference in the row-wise sum of the signed difference matrix and in the betweenness are provided for residues involved in EP2 or EP3 activation for all receptors. These individual residues mirror the general betweenness trends described above, with increases for EP1, no change for EP2, and decreases for EP3

Table 2. Difference in the Row-Wise Sum of the DNTE Signed Difference Matrix (SGN) and Difference in Betweenness Centrality upon PGE2 Binding for Residues Involved in the Hydrophobic Contact and Toggle Switch Activation Mechanisms for EP2 and EP3, Respectively

Residues involved in activation for	Residues binding to		
	Residues	ΔRow-wise sum of SGN	ΔBetweenness centrality
	EP1		
EP2[a] (hydrophobic contacts)	$L125^{3.40}$	−24	179.15
	$L215^{5.49}$	−103	167.31
	$S306^{6.44}$	−148	271.76
	$A340^{7.41}$	−218	127.65
EP3[b] (toggle switch)	$S209^{5.43}$	132	16.57
	$W310^{6.48}$	−135	346.98
	$M313^{6.51}$	−9	102.73
	EP2		
EP2[a] (hydrophobic contacts)	$M124^{3.40}$	−7	2.19
	$I208^{5.49}$	64	−4.90
	$F273^{6.44}$	−84	214.30
	$L304^{7.41}$	−184	58.12
EP3[b] (toggle switch)	$T202^{5.43}$	119	15.33
	$S277^{6.48}$	−103	−27.09
	$F280^{6.51}$	−32	−30.85
	EP3		
EP2[a] (hydrophobic contacts)	$L145^{3.40}$	152	−128.16
	$L240^{5.49}$	78	−106.45
	$L291^{6.44}$	−12	−133.27
	$A335^{7.41}$	31	−98.52
EP3[b] (toggle switch)	$F234^{5.43}$	101	−197.18
	$W295^{6.48}$	86	−136.54
	$L298^{6.51}$	104	−115.02

[a]Identified in ref 9. [b]Iidentified in ref 7.

https://doi.org/10.1021/acsabm.2c01049
ACS Appl. Bio Mater. XXXX, XXX, XXX−XXX

upon ligand binding. In the case of EP3, the difference in the row-wise sum of the signed difference matrix is positive for the toggle switch residues proposed in the literature (involving W295$^{6.48}$, F234$^{5.43}$, and L298$^{6.51}$) and the betweenness decreases. The decrease in betweenness indicates that as the residues involved in the switch become more driving in terms of information transfer, they can actually be described as more *directing* in that fewer information transfer pathways pass through the residues. In other words, only specific information is passing through these residues. On the other hand, in the case of EP2, the difference in the row-wise sum of the signed difference matrix is mostly negative for residues involved in activation (M124$^{3.40}$, I208$^{5.49}$, F273$^{6.44}$, L304$^{7.41}$) and the betweenness increases. These residues become more responding upon PGE_2 binding, however the increase in betweenness indicates that more information is transferred through these residues. In other words, the residues become more *mediating*, that is, they are able to initiate receptor activation via information transferred from other surrounding residues.

Interestingly, while EP1 has a conserved W310$^{6.48}$ toggle switch that would lead us to expect a similar activation mechanism to EP3, the information transfer signatures in EP1 are more similar to the hydrophobic contact mechanism observed in EP2. As a result, we predict that EP1 activation occurs via a slightly different mechanism than in EP3. While for EP3 the toggle switch directs information transfer to other residues upon interaction with PGE_2, we expect that in EP1, PGE_2 will transfer information to the toggle switch via multiple pathways, which will then result in receptor activation. From a molecular-level perspective, we observe that PGE_2 has contacts (with heavy atoms $\lesssim$3 Å apart) with EP3 W295$^{6.48}$ for 63% of the 500 ns simulation but only contacts EP3 W310$^{6.48}$ for 8% of the 500 ns simulation. These observations support the proposed differences in activation mechanism for EP1 compared to EP3.

CONCLUSIONS

In this study, molecular dynamics simulations of Prostaglandin E receptors are analyzed using a transfer entropy approach in order to understand molecular-level interactions that lead to activation upon PGE_2 binding. Three EP receptors were considered in this work: EP1, EP2, and EP3. The PGE_2 ligand was shown to interact with experimentally identified residues throughout the simulations. TE analysis revealed that key residues switch their information transfer behavior upon ligand binding. Most key residues switch their behavior from driving information transfer to responding to information upon ligand binding. For example, R$^{7.40}$, a key residue that forms hydrogen bonds with the PGE_2 carboxyl group, switches from driving to responding, but M$^{3.32}$, a residue that interacts with the hydrophobic ω chain, switches from responding to driving. In general, residues near the PGE_2 binding site (extracellular end) in TM1, TM2, and TM7 switch to responding, while those in TM3, TM4, TM5, and TM6 switch to driving. The betweenness centrality of the TE matrix was also considered in order to obtain a molecular-level description of how the information pathways change upon ligand binding, where increasing betweenness indicates more information pathways pass through that residue.

In particular, we aimed to obtain information regarding the activation mechanism in EP1, for which there is no experimental structure. Two activation mechanisms were considered, the W$^{6.48}$ toggle switch mechanism known in EP3,[7,10] as well as the hydrophobic contact mechanism known in EP2.[9] The W$^{6.48}$ toggle switch is present in both EP1 and EP3; however, the TE signatures observed from the simulations suggest differences in the specific activation mechanism. In EP3, the residues involved in the toggle switch mechanism become more directing upon PGE_2 binding, that is, they become more driving of information transfer, but their betweenness centrality decreases, indicating fewer information transfer pathways pass through the residues. On the other hand, in EP2, the residues involved in activation become more mediating upon PGE_2 binding. These residues become more responding to information transfer, but their betweenness increases, which indicates that although they can initiate activation, it likely involves receiving information from other residues.

In the case of EP1, we observe differences in mechanism and ligand contact between the toggle W$^{6.48}$ in EP1 and EP3. Whereas toggle switch residues become more directing in EP3, the corresponding residues in EP1 become more mediating. These results suggest that structural information on EP1 might reveal the toggle W$^{6.48}$ positioned differently from EP3. However, recent work by Pegram et al. highlights the complexity in structure/dynamic relationships, where they showed that two drug compounds can bind to a kinase in crystallographically indistinguishable poses but have exactly opposite effects on the conformational dynamics by NMR.[58] Thus, even if a structure shows good alignment between W$^{6.48}$ in EP1 and EP3, our results predict these receptors may still operate by different mechanisms. The mechanistic implications of driving vs mediating residues for drug design are an active area of research.[20,59] As these results indicate, using transfer entropy approaches to elucidate the distinct activation mechanisms in prostaglandin receptors is informative for establishing protein−ligand interaction and communication pathways. Thus, these results will be useful for future drug design targeting the human PGE2 receptors, and potentially other GPCRs as well.

ASSOCIATED CONTENT

Supporting Information

The Supporting Information is available free of charge at https://pubs.acs.org/doi/10.1021/acsabm.2c01049.

Force field parameters used for PGE2 ligand (TXT)

Complete structures of EP receptors, Alignment RMSD between AlphaFold structures and experimental structures, BW numbering scheme for EP receptors, Energy plots for the simulated system during production run, Plots of rms fluctuations of alpha carbons for each EP receptor, Plots of convergence of variance-covariance matrices for each EP receptor, List of relevant residue contacts during ligand binding, Plots of direct transfer entropy for each EP receptor, Plots of betweenness centrality of transfer entropy matrix for each EP receptor. (PDF)

AUTHOR INFORMATION

Corresponding Authors

Daniel A. Barr − *Department of Chemistry, University of Mary, Bismarck, North Dakota 58504, United States;* orcid.org/0000-0003-4660-5649; Email: dabarr@umary.edu

Heidi P. Hendrickson − *Department of Chemistry, Lafayette College, Easton, Pennsylvania 18042, United States;* orcid.org/0000-0002-5012-738X; Email: hendrihe@lafayette.edu

https://doi.org/10.1021/acsabm.2c01049
ACS Appl. Bio Mater. XXXX, XXX, XXX−XXX

Dhara J. Trivedi − *Department of Physics, Clarkson University, Potsdam, New York 13699, United States;* orcid.org/0000-0002-8151-3929; Email: dtrivedi@clarkson.edu

Authors

Nam P. Vu − *Department of Chemistry, Lafayette College, Easton, Pennsylvania 18042, United States*

Luke Ali − *Department of Physics, Clarkson University, Potsdam, New York 13699, United States;* orcid.org/0000-0003-2090-0578

Theresa L. Chua − *Department of Chemistry, Lafayette College, Easton, Pennsylvania 18042, United States*

Complete contact information is available at: https://pubs.acs.org/10.1021/acsabm.2c01049

Author Contributions

⊥N. P. Vu and L. Ali contributed equally to the work

Notes

The authors declare no competing financial interest.

■ ACKNOWLEDGMENTS

DB thanks Sarah Symalla for assistance with the calculation method for betweenness centrality and for helpful conversations about interpreting paths of information flow. Research reported in this publication was supported by an Institutional Development Award (IDeA) from the National Institute of General Medical Sciences of the National Institutes of Health under grant number P20GM103442. N.P.V., L.A., T.L.C., and H.P.H. thank Dr. Jason Simms and Peter Goode at the Lafayette College High Performance Computing Center for computational support. Computational resources were provided in part by the MERCURY consortium (mercuryconsortium.org/) under NSF Grants CHE-1229354 and CHE-1662030. DJT gratefully acknowledges Dr. Shikha Nangia and Dr. Shu Wang for the invitation to submit this manuscript.

■ REFERENCES

(1) Hirata, T.; Narumiya, S. Prostanoid Receptors. *Chem. Rev.* **2011**, *111* (10), 6209−6230.

(2) Markovič, T.; Jakopin, Ž.; Dolenc, M. S.; Mlinarič-Raščan, I. Structural Features of Subtype-Selective EP Receptor Modulators. *Drug Discovery Today* **2017**, *22* (1), 57−71.

(3) Woodward, D. F.; Jones, R. L.; Narumiya, S. International Union of Basic and Clinical Pharmacology. LXXXIII: Classification of Prostanoid Receptors, Updating 15 Years of Progress. *Pharmacol. Rev.* **2011**, *63* (3), 471.

(4) Venkatakrishnan, A. J.; Deupi, X.; Lebon, G.; Tate, C. G.; Schertler, G. F.; Babu, M. M. Molecular Signatures of G-Protein-Coupled Receptors. *Nature* **2013**, *494* (7436), 185−194.

(5) Rosenbaum, D. M.; Rasmussen, S. G. F.; Kobilka, B. K. The Structure and Function of G-Protein-Coupled Receptors. *Nature* **2009**, *459* (7245), 356−363.

(6) Toyoda, Y.; Morimoto, K.; Suno, R.; Horita, S.; Yamashita, K.; Hirata, K.; Sekiguchi, Y.; Yasuda, S.; Shiroishi, M.; Shimizu, T.; Urushibata, Y.; Kajiwara, Y.; Inazumi, T.; Hotta, Y.; Asada, H.; Nakane, T.; Shiimura, Y.; Nakagita, T.; Tsuge, K.; Yoshida, S.; Kuribara, T.; Hosoya, T.; Sugimoto, Y.; Nomura, N.; Sato, M.; Hirokawa, T.; Kinoshita, M.; Murata, T.; Takayama, K.; Yamamoto, M.; Narumiya, S.; Iwata, S.; Kobayashi, T. Ligand Binding to Human Prostaglandin E Receptor EP4 at the Lipid-Bilayer Interface. *Nat. Chem. Biol.* **2019**, *15* (1), 18−26.

(7) Morimoto, K.; Suno, R.; Hotta, Y.; Yamashita, K.; Hirata, K.; Yamamoto, M.; Narumiya, S.; Iwata, S.; Kobayashi, T. Crystal Structure of the Endogenous Agonist-Bound Prostanoid Receptor EP3. *Nat. Chem. Biol.* **2019**, *15* (1), 8−10.

(8) Nojima, S.; Fujita, Y.; Kimura, K. T.; Nomura, N.; Suno, R.; Morimoto, K.; Yamamoto, M.; Noda, T.; Iwata, S.; Shigematsu, H.; Kobayashi, T. Cryo-EM Structure of the Prostaglandin E Receptor EP4 Coupled to G Protein. *Structure* **2021**, *29* (3), 252−260.

(9) Qu, C.; Mao, C.; Xiao, P.; Shen, Q.; Zhong, Y.-N.; Yang, F.; Shen, D.-D.; Tao, X.; Zhang, H.; Yan, X.; Zhao, R.-J.; He, J.; Guan, Y.; Zhang, C.; Hou, G.; Zhang, P.-J.; Hou, G.; Li, Z.; Yu, X.; Chai, R.-J.; Guan, Y.-F.; Sun, J.-P.; Zhang, Y. Ligand Recognition, Unconventional Activation, and G Protein Coupling of the Prostaglandin E $_2$ Receptor EP2 Subtype. *Sci. Adv.* **2021**, *7* (14), No. eabf1268.

(10) Trzaskowski, B.; Latek, D.; Yuan, S.; Ghoshdastider, U.; Debinski, A.; Filipek, S. Action of Molecular Switches in GPCRs - Theoretical and Experimental Studies. *Curr. Med. Chem.* **2012**, *19* (8), 1090−1109.

(11) Minami, T.; Nakano, H.; Kobayashi, T.; Sugimoto, Y.; Ushikubi, F.; Ichikawa, A.; Narumiya, S.; Ito, S. Characterization of EP Receptor Subtypes Responsible for Prostaglandin E2-induced Pain Responses by Use of EP1 and EP3 Receptor Knockout Mice. *Br. J. Pharmacol.* **2001**, *133* (3), 438−444.

(12) Cimino, P.; Keene, C. D.; Breyer, R. M.; Montine, K. S.; Montine, T. J. Therapeutic Targets in Prostaglandin E2 Signaling for Neurologic Disease. *Curr. Med. Chem.* **2008**, *15* (19), 1863−1869.

(13) Legler, D. F.; Bruckner, M.; Uetz-von Allmen, E.; Krause, P. Prostaglandin E2 at New Glance: Novel Insights in Functional Diversity Offer Therapeutic Chances. *Int. J. Biochem. Cell Biol.* **2010**, *42* (2), 198−201.

(14) Breyer, R. M.; Bagdassarian, C. K.; Myers, S. A.; Breyer, M. D. Prostanoid Receptors: Subtypes and Signaling. *Annu. Rev. Pharmacol. Toxicol.* **2001**, *41* (1), 661−690.

(15) Alakent, B.; Ince, Z. N. G. *Elucidating Allosteric Communication in Proteins via Computational Methods*; Bentham Science Publishers: Sharjah, UAE, 2017; Vol. 3.

(16) Garcia Michel, L. R.; Keirns, C. D.; Ahlbrecht, B. C.; Barr, D. A. Calculating Transfer Entropy from Variance−Covariance Matrices Provides Insight into Allosteric Communication in ERK2. *J. Chem. Theory Comput.* **2021**, *17* (5), 3168−3177.

(17) Schreiber, T. Measuring Information Transfer. *Phys. Rev. Lett.* **2000**, *85* (2), 461−464.

(18) Kamberaj, H.; van der Vaart, A. Extracting the Causality of Correlated Motions from Molecular Dynamics Simulations. *Biophys. J.* **2009**, *97* (6), 1747−1755.

(19) Hacisuleyman, A.; Erman, B. Information Flow and Allosteric Communication in Proteins. *J. Chem. Phys.* **2022**, *156* (18), 185101.

(20) Madhu, M. K.; Debroy, A.; Murarka, R. K. Molecular Insights into Phosphorylation-Induced Allosteric Conformational Changes in a B2-Adrenergic Receptor. *J. Phys. Chem. B* **2022**, *126* (9), 1917−1932.

(21) Narumiya, S.; Sugimoto, Y.; Ushikubi, F. Prostanoid Receptors: Structures, Properties, and Functions. *Physiol. Rev.* **1999**, *79* (4), 1193−1226.

(22) Konya, V.; Marsche, G.; Schuligoi, R.; Heinemann, A. E-Type Prostanoid Receptor 4 (EP4) in Disease and Therapy. *Pharmacol. Ther.* **2013**, *138* (3), 485−502.

(23) Biringer, R. G. A Review of Prostanoid Receptors: Expression, Characterization, Regulation, and Mechanism of Action. *J. Cell Commun. Signal.* **2021**, *15* (2), 155−184.

(24) Bazzani, L.; Donnini, S.; Finetti, F.; Christofori, G.; Ziche, M. PGE2/EP3/SRC Signaling Induces EGFR Nuclear Translocation and Growth through EGFR Ligands Release in Lung Adenocarcinoma Cells. *Oncotarget* **2017**, *8* (19), 31270.

(25) Jumper, J.; Evans, R.; Pritzel, A.; Green, T.; Figurnov, M.; Ronneberger, O.; Tunyasuvunakool, K.; Bates, R.; Žídek, A.; Potapenko, A.; Bridgland, A.; Meyer, C.; Kohl, S. A. A.; Ballard, A. J.; Cowie, A.; Romera-Paredes, B.; Nikolov, S.; Jain, R.; Adler, J.; Back, T.; Petersen, S.; Reiman, D.; Clancy, E.; Zielinski, M.; Steinegger, M.; Pacholska, M.; Berghammer, T.; Bodenstein, S.; Silver, D.; Vinyals, O.; Senior, A. W.; Kavukcuoglu, K.; Kohli, P.; Hassabis, D. Highly Accurate Protein Structure Prediction with AlphaFold. *Nature* **2021**, *596* (7873), 583−589.

(26) Varadi, M.; Anyango, S.; Deshpande, M.; Nair, S.; Natassia, C.; Yordanova, G.; Yuan, D.; Stroe, O.; Wood, G.; Laydon, A.; Žídek, A.; Green, T.; Tunyasuvunakool, K.; Petersen, S.; Jumper, J.; Clancy, E.; Green, R.; Vora, A.; Lutfi, M.; Figurnov, M.; Cowie, A.; Hobbs, N.; Kohli, P.; Kleywegt, G.; Birney, E.; Hassabis, D.; Velankar, S. AlphaFold Protein Structure Database: Massively Expanding the Structural Coverage of Protein-Sequence Space with High-Accuracy Models. *Nucleic Acids Res.* **2022**, *50* (D1), D439−D444.
(27) Pándy-Szekeres, G.; Esguerra, M.; Hauser, A. S.; Caroli, J.; Munk, C.; Pilger, S.; Keserű, G. M.; Kooistra, A. J.; Gloriam, D. E. The G Protein Database, GproteinDb. *Nucleic Acids Res.* **2022**, *50* (D1), D518−D525.
(28) Ballesteros, J. A.; Weinstein, H. [19] Integrated Methods for the Construction of Three-Dimensional Models and Computational Probing of Structure-Function Relations in G Protein-Coupled Receptors. In *Methods in Neurosciences*; Elsevier, 1995; Vol. *25*, pp 366−428. DOI: 10.1016/S1043-9471(05)80049-7.
(29) Dickson, C. J.; Walker, R. C.; Gould, I. R. Lipid21: Complex Lipid Membrane Simulations with AMBER. *J. Chem. Theory Comput.* **2022**, *18* (3), 1726−1736.
(30) Izadi, S.; Anandakrishnan, R.; Onufriev, A. V. Building Water Models: A Different Approach. *J. Phys. Chem. Lett.* **2014**, *5* (21), 3863−3871.
(31) Schott-Verdugo, S.; Gohlke, H. PACKMOL-Memgen: A Simple-To-Use, Generalized Workflow for Membrane-Protein−Lipid-Bilayer System Building. *J. Chem. Inf. Model.* **2019**, *59* (6), 2522−2528.
(32) *PyMOL Molecular Graphics System*, Version 2.0.
(33) Frisch, M. J.; Trucks, G. W.; Schlegel, H. B.; Scuseria, G. E; Robb, M. A.; Cheeseman, J. R.; Scalmani, G.; Barone, V.; Petersson, G. A.; Nakatsuji, H.; Li, X.; Caricato, M.; Marenich, A. V.; Bloino, J.; Janesko, B. G.; Gomperts, R.; Mennucci, B.; Hratchian, H. P.; Ortiz, J. V.; Izmaylov, A. F.; Sonnenberg, J. L.; Williams-Young, D.; Ding, F.; Lipparini, F.; Egidi, F.; Goings, J.; Peng, B.; Petrone, A.; Henderson, T.; Ranasinghe, D.; Zakrzewski, V. G.; Gao, J.; Rega, N.; Zheng, G.; Liang, W.; Hada, M.; Ehara, M.; Toyota, K.; Fukuda, R.; Hasegawa, J.; Ishida, M.; Nakajima, T.; Honda, Y.; Kitao, O.; Nakai, H.; Vreven, T.; Throssell, K.; Montgomery, J. A., Jr.; Peralta, J. E.; Ogliaro, F.; Bearpark, M. J.; Heyd, J. J.; Brothers, E. N.; Kudin, K. N.; Staroverov, V. N.; Keith, T. A.; Kobayashi, R.; Normand, J.; Raghavachari, K.; Rendell, A. P.; Burant, J. C.; Iyengar, S. S.; Tomasi, J.; Cossi, M.; Millam, J. M.; Klene, M.; Adamo, C.; Cammi, R.; Ochterski, J. W.; Martin, R. L.; Morokuma, K.; Farkas, O.; Foresman, J. B.; Fox, D. J. *Gaussian 16, Revision B.01*, 2016.
(34) Dennington, R.; Keith, T. A.; Millam, J. M. *GaussView 6.0.16*, 2016.
(35) Wang, J.; Wang, W.; Kollman, P. A.; Case, D. A. Automatic Atom Type and Bond Type Perception in Molecular Mechanical Calculations. *J. Mol. Graph. Model.* **2006**, *25* (2), 247−260.
(36) Wang, J.; Wolf, R. M.; Caldwell, J. W.; Kollman, P. A.; Case, D. A. Development and Testing of a General Amber Force Field. *J. Comput. Chem.* **2004**, *25* (9), 1157−1174.
(37) Case, D. A.; Aktulga, H. M.; Belfon, K.; Ben-Shalom, I. Y.; Berryman, J. T.; Brozell, S. R.; Cerutti, D. S.; Cheatham, T. E., III; Cisneros, G. A.; Cruzeiro, V. W. D.; Darden, T. A.; Duke, R. E.; Giambasu, G.; Gilson, M. K.; Gohlke, H.; Goetz, A. W.; Harris, R.; Izadi, S.; Izmailov, S. A.; Kasavajhala, K.; Kaymak, M. C.; King, E.; Kovalenko, A.; Kurtzman, T.; Lee, T. S.; LeGrand, S.; Li, P.; Lin, C.; Liu, J.; Luchko, T.; Luo, R.; Machado, M.; Man, V.; Manathunga, M.; Merz, K. M.; Miao, Y.; Mikhailovskii, O.; Monard, G.; Nguyen, H.; O'Hearn, K. A.; Onufriev, A.; Pan, F.; Pantano, S.; Qi, R.; Rahnamoun, A.; Roe, D. R.; Roitberg, A.; Sagui, C.; Schott-Verdugo, S.; Shajan, A.; Shen, J.; Simmerling, C. L.; Skrynnikov, N. R.; Smith, J.; Swails, J.; Walker, R. C.; Wang, J.; Wang, J.; Wei, H.; Wolf, R. M.; Wu, X.; Xiong, Y.; Xue, Y.; York, D. M.; Zhao, S.; Kollman, P. A. *Amber 2022*, 2022.
(38) Tian, C.; Kasavajhala, K.; Belfon, K. A. A.; Raguette, L.; Huang, H.; Migues, A. N.; Bickel, J.; Wang, Y.; Pincay, J.; Wu, Q.; Simmerling, C. Ff19SB: Amino-Acid-Specific Protein Backbone Parameters Trained against Quantum Mechanics Energy Surfaces in Solution. *J. Chem. Theory Comput.* **2020**, *16* (1), 528−552.
(39) Dickson, C. J. *AMBER Membrane Protein Tutorial*, 2022. https://github.com/callumjd/AMBER-Membrane_protein_tutorial.
(40) Hopkins, C. W.; Le Grand, S.; Walker, R. C.; Roitberg, A. E. Long-Time-Step Molecular Dynamics through Hydrogen Mass Repartitioning. *J. Chem. Theory Comput.* **2015**, *11* (4), 1864−1874.
(41) Ryckaert, J.-P.; Ciccotti, G.; Berendsen, H. J. C. Numerical Integration of the Cartesian Equations of Motion of a System with Constraints: Molecular Dynamics of n-Alkanes. *J. Comput. Phys.* **1977**, *23* (3), 327−341.
(42) Roe, D. R.; Cheatham, T. E. I. PTRAJ and CPPTRAJ: Software for Processing and Analysis of Molecular Dynamics Trajectory Data. *J. Chem. Theory Comput.* **2013**, *9* (7), 3084−3095.
(43) Humphrey, W.; Dalke, A.; Schulten, K. VMD: Visual Molecular Dynamics. *J. Mol. Graph.* **1996**, *14* (1), 33−38.
(44) Michaud-Agrawal, N.; Denning, E. J.; Woolf, T. B.; Beckstein, O. MDAnalysis: A Toolkit for the Analysis of Molecular Dynamics Simulations. *J. Comput. Chem.* **2011**, *32* (10), 2319−2327.
(45) Gowers, R.; Linke, M.; Barnoud, J.; Reddy, T.; Melo, M.; Seyler, S.; Domański, J.; Dotson, D.; Buchoux, S.; Kenney, I.; Beckstein, O. MDAnalysis: A Python Package for the Rapid Analysis of Molecular Dynamics Simulations; Austin. *Texas* **2016**, 98−105.
(46) *Flare*, 2022. http://www.cresset-group.com/flare/.
(47) Cheeseright, T.; Mackey, M.; Rose, S.; Vinter, A. Molecular Field Extrema as Descriptors of Biological Activity: Definition and Validation. *J. Chem. Inf. Model.* **2006**, *46* (2), 665−676.
(48) Bauer, M. R.; Mackey, M. D. Electrostatic Complementarity as a Fast and Effective Tool to Optimize Binding and Selectivity of Protein−Ligand Complexes. *J. Med. Chem.* **2019**, *62* (6), 3036−3050.
(49) Kuhn, M.; Firth-Clark, S.; Tosco, P.; Mey, A. S. J. S.; Mackey, M.; Michel, J. Assessment of Binding Affinity via Alchemical Free-Energy Calculations. *J. Chem. Inf. Model.* **2020**, *60* (6), 3120−3130.
(50) Welford, B. P. Note on a Method for Calculating Corrected Sums of Squares and Products. *Technometrics* **1962**, *4* (3), 419−420.
(51) Barr, D.; Oashi, T.; Burkhard, K.; Lucius, S.; Samadani, R.; Zhang, J.; Shapiro, P.; MacKerell, A. D.; van der Vaart, A. Importance of Domain Closure for the Autoactivation of ERK2. *Biochemistry* **2011**, *50* (37), 8038−8048.
(52) Kamberaj, H. Sampling Convergence Of Collective Motions In Proteins. *J. Appl. Phys. Sci. Int.* **2017**, 101−112.
(53) Hacisuleyman, A.; Erman, B. Causality, Transfer Entropy, and Allosteric Communication Landscapes in Proteins with Harmonic Interactions. *Proteins Struct. Funct. Bioinforma.* **2017**, *85* (6), 1056−1064.
(54) Novelli, L.; Lizier, J. T. Inferring Network Properties from Time Series Using Transfer Entropy and Mutual Information: Validation of Multivariate versus Bivariate Approaches. *Netw. Neurosci.* **2021**, *5* (2), 373−404.
(55) Novelli, L.; Atay, F. M.; Jost, J.; Lizier, J. T. Deriving Pairwise Transfer Entropy from Network Structure and Motifs. *Proc. R. Soc. Math. Phys. Eng. Sci.* **2020**, *476* (2236), 20190779.
(56) Wolfram Research, Inc. *Mathematica*, 2022. https://www.wolfram.com/mathematica.
(57) Chang, C.; Negishi, M.; Nishigaki, N.; Ichikawa, A. Of Functional Intheraction of Carboxylic Acid Groupof Agonists and Argininеof the SeventhTransmembrane Domains of Four ProstaglandinE Receptor Subtypes. *Prostaglandins* **1997**, *54*, 437−446.
(58) Pegram, L. M.; Liddle, J. C.; Xiao, Y.; Hoh, M.; Rudolph, J.; Iverson, D. B.; Vigers, G. P.; Smith, D.; Zhang, H.; Wang, W.; Moffat, J. G.; Ahn, N. G. Activation Loop Dynamics Are Controlled by Conformation-Selective Inhibitors of ERK2. *Proc. Natl. Acad. Sci. U. S. A.* **2019**, *116* (31), 15463−15468.
(59) Maschietto, F.; Gheeraert, A.; Piazzi, A.; Batista, V. S.; Rivalta, I. Distinct Allosteric Pathways in Imidazole Glycerol Phosphate Synthase from Yeast and Bacteria. *Biophys. J.* **2022**, *121* (1), 119−130.

https://doi.org/10.1021/acsabm.2c01049
ACS Appl. Bio Mater. XXXX, XXX, XXX−XXX